RSC Advances

PAPER

View Article Online
View Journal | View Issue

Cite this: *RSC Adv.*, 2015, **5**, 88590

Zinc titanium glycolate acetate hydrate and its transformation to zinc titanate microrods: synthesis, characterization and photocatalytic properties†

Guo-Hui Pan,*[ab] Tomokatsu Hayakawa,[b] Masayuki Nogami,*[b] Zhendong Hao,[a] Xia Zhang,[a] Xuesong Qu[c] and Jiahua Zhang*[a]

A heterobimetallic complex, zinc titanium glycolate acetate hydrate (Zn_2Ti_3–GAH), tentatively formulated as $Zn_2Ti_3(OCH_2CH_2O)_4(OCH_2CH_2OH)_5(CH_3COO)_3\cdot 2HOCH_2CH_2OH\cdot H_2O$, was synthesized by a room-temperature homogeneous precipitation in ethylene glycol solution. Its chemical composition, crystal structure, morphology, growth mechanism and thermal behaviors were characterized in detail. The precipitated Zn_2Ti_3–GAH was of a highly crystalline monoclinic phase and porous microrod morphology. As the single source precursor (SSP), Zn_2Ti_3–GAH was transformed into different phases of zinc titanate *via* thermal decomposition. With the remaining shape of the microrods, cubic phases of $Zn_2Ti_3O_8$ and rutile TiO_2 (r-TiO_2) supported hexagonal phases of $ZnTiO_3$ (h-$ZnTiO_3$) were obtained by calcination at 500 and 700 °C, respectively; while r-TiO_2 supported Zn_2TiO_4 were yielded in the form of dispersed particles or chains at higher temperature (950 °C). Benefiting from the SSP route and the confinement in the specific microrod domains of precursors, the heterostructures of r-TiO_2–$ZnTiO_3$ and r-TiO_2–Zn_2TiO_4 were formed during programmable calcination. The studies on photocatalysis by degrading methylene blue (MB) under ultraviolet (UV) irradiation indicated that the as-transformed zinc titanate exhibited enhanced activity. In particular, r-TiO_2 supported h-$ZnTiO_3$ displayed the photodegradation reaction rate constant of 0.00163 s^{-1}, which was comparable to that of commercially available Degussa P25 TiO_2. This probably related to the more effective charge separation in the r-TiO_2–$ZnTiO_3$ heterostructure packed in the microrods.

Received 7th September 2015
Accepted 6th October 2015

DOI: 10.1039/c5ra18292a

www.rsc.org/advances

1. Introduction

Over the past few decades, there has been a growing interest in novel heterometallic complexes due to their capability as molecular single source precursors (SSP) to advanced doped metal oxides and mixed-metal oxides *via* chemical routes (*e.g.* sol–gel techniques).[1–9] Such conversions generally feature a processing of well-defined stoichiometric ratio of the metal elements on the molecular level and at relatively low temperatures. The resulting oxides usually inherit some structural features of synthetic precursors.[10] Synthesis of new heterometallic complexes holding unique structures and properties is of great significance for the investigation of sol–gel processes as well as the evolution of metal alkoxide chemistry.[10] Of particular interest is titanium based heterometallic complexes for their great potential in photocatalysts, photovoltaic cells, electroceramics and many others.[7–9]

The coordination systems of heterometallic complexes are mainly stabilized by alkoxo-bridges, polyolates chelating ligands and oxo ligands between different metal atoms,[4] which could be accordingly termed as heterometallic alkoxides, heterometallic polyolate-alkoxides and heterometallic polyoxometallate, respectively. Heterometallic alkoxides were investigated much earlier.[1,2] Examples of titanium containing heterometallic alkoxides such as $[M\{Ti(OR)_5\}]_n$ (M = Li, Na, K), $[Mg\{Ti_2(OEt)_8Cl\}(\mu\text{-}Cl)]_2$, $Cd\{Ti_2(O^iPr)_9\}I$, $[\{Cd(O^iPr)_3\}Ba$

[a]*State Key Laboratory of Luminescence and Applications, Changchun Institute of Optics, Fine Mechanics and Physics, Chinese Academy of Sciences, 3888 Dong Nanhu Road, Changchun 130033, China. E-mail: guohui.pan@aliyun.com; zhangjh@ciomp.ac.cn*

[b]*Department of Materials Science and Engineering, Nagoya Institute of Technology, Showa, Nagoya 466-8555, Japan. E-mail: mnogami@mtj.biglobe.ne.jp*

[c]*Department of Physics, Changchun Normal University, Changchun 130032, China*

† Electronic supplementary information (ESI) available: FTIR spectrum, XRD pattern, N_2 adsorption–desorption isotherm at 77 K, TEM-EDS spectrum, CPMAS ^{13}C NMR spectrum and solution ^1H and ^{13}C NMR spectra of zinc titanium glycolate acetate hydrate (Zn_2Ti_3–GAH) or other samples; XRD patterns and SEM images of Zn_2Ti_3–GAH after immersing in DMSO, DMF and H_2O overnight; MS comparisons of the experimentally obtained isotopic distribution pattern with the calculated pattern of molecule ion peaks of other species detected after treating Zn_2Ti_3–GAH with DMF; the TG curve of Zn_2Ti_3–GAH in temperature range of 25–300 °C for showing the point of inflection between step 1 and 2 during thermal evolution; SEM images of products by sampling at different periods of reaction time when synthesizing Zn_2Ti_3–GAH; determination of the band gaps of Zn_2Ti_3–GAH and zinc titanate *via* thermal treatment at varied temperature. See DOI: 10.1039/c5ra18292a

$\{Ti_2(O^iPr)_9\}]_2$ and $M_2Ti_2(OR)_x(acac)_y$ (M = Mg, Co^{II}, Ni) were synthesized through reactions involving union of two different metal alkoxides or reactions of titanium alkoxides $Ti(OR)_4$ (R = alkyl) and alkali metal alkoxotitanate ligands with metal halides or acetylacetonates (acac);[1,2,11] Some novel types of heterobimetallic polyolate-alkoxides derived from various polyols (glycols, di- and tri-ethanolamines ($teaH_3$) with common formulas of $M_xTi(OGO)_y(O^iPr)_z(HOGOH)_n$ (M = Ce, Ta, Al, K, Na, Zr; G = CH_2CH_2, CMe_2CMe_2, $CHMeCH_2CMe_2$, $CMe_2CH_2CH_2$-CMe_2) and $M_xTi_y(A)_z(OR)_n$ (M = Mg, Ca, Sr, Ba, Al, Ta, Nb; A = diethanolaminate (2-), triethanolaminate (3-); R = ^{i}Pr, ^{t}Bu), *etc.*, were generally obtained by the interactions of residual hydroxyl groups in the pre-formed homometallic derivatives (titanium polyolates) with alkoxides of other metals.[3,4,9] More recently, a variety of heterobimetallic polyoxotitanate cage compounds with a general formulae of $[Ti_xO_y(OR)_zM_nL_m]$ (M = La, Ce, Nd, Eu, Ga, Co^{II}, Zn, Fe^{II}, Cu, Ni, Mn^{II}, Mo^{v}, Cr^{v}, *etc.*; L = Cl, Br, I, HO^iPr, McOH (Methacrylic acid), *etc.*) were synthesized by a well-controlled solvothermal method *via* a reaction of $Ti(OR)_4$ or the pre-formed homometallic titanium-oxo-alkoxy cage with metal chlorides, hydrated metal acetates and hydrated metal sulfates.[5–8,12–19] Synthesis at room temperature, however, was less reported.[19] Organically-soluble crystals are frequently obtained during the solvothermal heating–cooling cycle or during *a posteriori* partial evaporation of the mother liquor.[7] In particular, in the absence of the above mentioned stabilizing ligands U. Schubert *et al.* recently synthesized the Zn–Ti–POBC bimetallic complex by means of a bifunctional linker of *p*-carboxybenzaldehyde oxime (POBC-H) upon reacting $Ti(O^iPr)_4$ with $Zn(POBC)_2$.[20]

In this study, we reported on a heterobimetallic glycolate–acetate complex, zinc titanium glycolate acetate hydrate (Zn_2Ti_3–GAH) tentatively formulated as $Zn_2Ti_3(OCH_2CH_2O)_4$-$(OCH_2CH_2OH)_5(CH_3COO)_3\cdot 2HOCH_2CH_2OH\cdot H_2O$, through a facile room-temperature precipitation reaction in ethylene glycol (EG) solution, which started from ambient-stable titanium glycolate derivatives and zinc glycolate acetate species. Similar EG mediated routes were previously described by H. Fu *et al.* to synthesize Zn–Ti, Ni–Ti and Co–Ti heterobimetallic glycolate precursors, though full understanding of their chemical compositions and structures was lacked.[21–23] Herein these concerns were detailed on the basis of various analysis techniques. The as-precipitated Zn_2Ti_3–GAH appeared as highly crystalline monoclinic phase and porous microrods morphology. It thermally decomposed into different crystallographic phase of ZnO–TiO_2 system from phase-pure $Zn_2Ti_3O_8$ (cubic, defect-spinel type, porous microrods), then to rutile TiO_2 supported $ZnTiO_3$ (hexagonal, ilmenite-type, porous microrods) and finally to rutile TiO_2 supported Zn_2TiO_4 (cubic, spinel-type, microcrystallites). Of particular interest is $ZnTiO_3$ as promising dielectric materials for capacitors or microwave devices,[24–31] gas sensors,[32] paint pigments,[27,33] and novel luminescent host.[24,34–36] Zn_2TiO_4 was attractive as regenerable sorbents for catalytic desulphurization and dehydrogenation of hot gas.[37,38] $Zn_2Ti_3O_8$ was recently demonstrated as the anode material for rechargeable lithium-ion battery and photocatalyst for water splitting.[22,39] The work presented herein evaluated their photocatalytic performance against degradation of methylene blue (MB) under UV irradiations. r-TiO_2 supported h-$ZnTiO_3$ displayed higher photocatalytic performance probably due to the presence of r-TiO_2–$ZnTiO_3$ heterostructure packed in microrods.

2. Experimental section

2.1 Chemicals

All chemicals were used as received without further purification. Titanium tetrabutoxide (TTB, $Ti(OC_4H_9)_4$, 99.9 wt%), ethylene glycol (EG, $HOCH_2CH_2OH$, A.R.), zinc acetate dihydrate ($Zn(CH_3COO)_2\cdot 2H_2O$, A.R.) and absolute ethanol were purchased from Kishida Chemical CO., LTD, Japan; *N*,*N*-dimethyl-formamide (DMF, A.R.) and dimethyl sulfoxide (DMSO, A.R.) were got from Xilong Chemical CO., LTD, China; methylene blue (MB) was bought from Aladdin Industrial Inc., China.

2.2 Synthesis of Zn_2Ti_3–GAH

All manipulations were carried out under ambient conditions. In a typical synthesis, 0.5 mL of TTB was added into 100 mL EG under magnetic stirring, which immediately became cloudy and gave *in situ* a clear, colorless solution of titanium glycolate precursors upon continuous stirring overnight. The titanium glycolate precursors were used in the following reaction without further isolation. 0.3216 g of zinc acetate dihydrate (with a Ti/Zn molar ratio of ~1 : 1) was dissolved in 20 mL of EG with stirring and then poured into the above solution. The reaction was allowed to proceed with stirring at room temperature. The first visible sign of the turbidity appeared in the clear solution ~1 h after the addition of zinc source and, then the solution gradually became more turbid. The whole homogeneous precipitation was completed in ~3 h, yielding a concentrated suspension. Afterward, stirring continued for 2 h followed by aging for ~12 h. White powders of Zn_2Ti_3–GAH (0.5733 g, ~95% yield with respect to $[Ti(OC_4H_9)_4]$ supplied) were collected from the solution by centrifugation, washed with ethanol, and finally dried at 60 °C for 12 h in air. Zn_2Ti_3–GAH was subjected to calcinations in a muffle furnace under static air at different temperature for different periods of time. The heating rate was ~8 °C min^{-1}.

To study the effects of Zn/Ti molar ratios of the precursors on the reaction process and precipitated products, additional synthesis with Zn : Ti = 2 : 3 and 1 : 2 was performed under otherwise constant conditions.

To check the stability of Zn_2Ti_3–GAH against humidity, DMF and DMSO, 40 mg of the as-obtained sample was suspended in 15 mL of water, DMSO and DMF overnight, respectively; they were then collected for structure and morphology characterizations from the solution by centrifugation, washed with ethanol, and finally dried at 60 °C for 12 h in air. In the case of DMF, the soaking experiments were performed two times on the same powders.

Zn_2Ti_3–GAH was poorly soluble in water and common organic solvents.

FT-IR (KBr, 4000–400 cm^{-1}): ν/cm^{-1} = 3425 br (ν_s(O–H) in EG and H_2O), 2926 s ($\nu_{as}(CH_2)$ C–CH_2), 2856 s ($\nu_s(CH_2)$ C–CH_2), 1665m (δ(H–O–H)), 1570m ($\nu_{as}(COO^-)$), 1420m, ($\nu_s(COO^-)$), 1391w ($\delta_{as}(CH_3)$), 1340w (β(O–H)), 1200–1270w (ν_{as}(–C–C–O–)), 1116w (C–O–Ti), 1074 *vs.* (ν_s(C–O), δ(C–O–H)), 1034m (δ(C–O)), 914m ($\gamma(CH_2)$), 885m ($\gamma(CH_2)$), 624 s (ν_s(Ti–O)), 563 s (ν_s(Ti–O)), 478 s (ν_s(Ti–O)).

Solid-state $^{13}C\{^1H\}$ NMR (100.63 MHz, +25 °C, ppm): δ = 74.130, 63.910, 61.295. Solution ^1H NMR (500.13 MHz, [D_6] DMSO, +25 °C, ppm): δ = 1.059 (t, J = 5 Hz, CH_3), 1.151 (s), 1.238(s, CH_3), 1.250 (s, CH_3), 2.016 (s, CCH_3), 2.524 (t, J = 2 Hz, CH_3), 3.256 (q, J = 5.5 Hz, OCH_2), 3.315 (s, OCH_2), 3.339 (s, OCH_2 and H_2O), 3.392 (t, J = 2.5 Hz, OCH_2), 3.523 (q, J = 5.5 Hz, OCH_2), 4.452 (p, J = 5.5 Hz, OCH_2); solution ^{13}C NMR (125.77 MHz, [D_6] DMSO, +25 °C, ppm): δ = 39.900, 40.066, 40.232, 40.399, 40.476, 40.567, 63.249 (OCH_2).

MS (m/z): calcd for 1273.22 ($C_{34}H_{81}O_{36}Ti_3Zn$, [M + H]$^+$), found: 1273.00; calcd for 1159.05 ($C_{28}H_{64}O_{29}Ti_3Zn_2Na$, [$M$ + Na]$^+$), found: 1158.93; calcd for 1137.06 ($C_{28}H_{65}O_{29}Ti_3Zn_2$, [$M$ + H]$^+$), found: 1136.95; calcd for 1113.30 ($C_{30}H_{81}O_{32}Ti_2Zn$, [M + H]$^+$), found: 1113.00; calcd for 943.12 ($C_{24}H_{56}O_{26}Ti_2ZnNa$, [$M$ + Na]$^+$), found: 942.85; calcd for 921.14 ($C_{24}H_{57}O_{26}Ti_2Zn$, [M + H]$^+$), found: 920.85; calcd for 807.07 ($C_{20}H_{48}O_{20}TiZn_2Na$, [$M$ + Na]$^+$), found: 806.90; calcd for 785.09 ($C_{20}H_{49}O_{20}TiZn_2$, [M + H]$^+$), found: 784.90; calcd for 727.16 ($C_{20}H_{48}O_{20}Ti_2Na$, [M + Na]$^+$), found: 726.93; calcd for 705.18 ($C_{20}H_{49}O_{20}Ti_2$, [M + H]$^+$), found: 704.93.

Elemental analysis (%): calcd for $C_{28}H_{64}O_{29}Ti_3Zn_2$: Zn 11.48, Ti 12.61, C 29.52, H 5.66; found: Zn 12.34, Ti, 12.10, C 27.29, H 5.86.

TGA/DTA: theoretical weight loss 64.8%, actual 66.7%. Thermal events (°C): 180w (*endo*), 214s (*exo*), 291s (*exo*), 370w (*exo*).

2.3 Photocatalytic activity measurements

The photocatalytic performance was evaluated through the decomposition of MB (methylene blue, 50 mL, 10 mg L^{-1} in H_2O) under ~29.2 mW cm^{-2} ultraviolet (UV, 253.7 nm) irradiation of a Hg lamp at room temperature in the presence of photocatalyst (50 mg). After being stirred in a well-shaped reactor 7.0 cm in caliber in the dark for 2 h to achieve the absorption–desorption equilibrium, the mixture was exposed to the UV light under constant stirring. For a given duration of 2 or 10 min, the change in the concentration of MB (after the removal of photocatalysts through centrifugation) was checked by its absorption evolution at 664 nm recorded on a UV-visible spectrophotometer (Shimadzu UV-2600). As controls, commercially available photocatalyst of Degussa P25 TiO_2 and MB aqueous solutions without any catalyst were also irradiated under otherwise the same conditions.

2.4 Characterization

2.4.1. Powder X-ray diffraction (XRD). XRD of the dried powder were recorded on a Philips X'pert diffractometer (Cu-Kα radiation, 1.54056 Å) with an applied voltage of 45 kV and 40 mA anode current over the 2θ range of 10–80°.

2.4.2. Scanning electron microscopy (SEM) and transmission electron microscopy (TEM). The SEM imaging was examined on a Hitachi S4800 microscope. TEM imaging, selective area electron diffraction (SAED) and energy dispersive X-ray spectra (EDS) were performed on a FEI Tecnai G2-F20 microscope operating at 200 kV.

2.4.3. Fourier transform infrared (FT-IR). FTIR spectra in the 400–4000 cm^{-1} range were obtained on a JASCO FTIR-460 Plus spectrometer, using the KBr pellet method.

2.4.4. Nuclear magnetic resonance (NMR). $^{13}C\{^1H\}$ solid-state NMR spectra were obtained on a Bruker AVANCE III 400 WB spectrometer at a frequency of 100.63 MHz using a 4 mm broadband magic angle spinning (MAS) probe, spinning at 8 kHz. Solution ^1H and ^{13}C NMR spectra were recorded at 298 K on a Bruker Avance III HD 500 MHz spectrometer, with working frequencies of 500.13 MHz for ^1H, and 125.77 MHz for ^{13}C nuclei, respectively.

2.4.5. Mass spectra (MS). Matrix-assisted laser desorption ionization time-of-flight (MALDI-TOF) mass spectrometry analyses were performed on Bruker autoflex III smartbeam MALDI-TOF/TOF mass spectrometer equipped with a Nd:YAG laser operating at 355 nm. The laser intensity was adjusted to obtain good resolution and signal-to-noise ratio (S/N). *N*,*N*-Dimethyl-formamide (DMF) was used as the solvent for the sample dispersion (1 mg mL^{-1}) and matrix of 2,5-dihydroxybenzoic acid (DHB) (20 mg mL^{-1}) helping ionization.

2.4.6. Thermogravimetric and differential thermal analyses (TG-DTA). The thermal behaviors were investigated by TG-DTA (Thermoplus 2, TG-8120, Rigaku) with a heating rate of 5 °C min^{-1} over a 20–1000 °C temperature range in air.

2.4.7. TG-FTIR. Simultaneous TG-FTIR experiments were conducted using a joint Mettler Toledo thermogravimetric analyzer (TGA/DSC 1 STAR^e System) and Thermo Scientific FTIR instrument (Nicolet iS10). A heating rate of 5 °C min^{-1} was used under a flowing air atmosphere in a temperature range of 32–750 °C.

2.4.8. Chemical analysis. The chemical analyses were carried out on inductively coupled plasma-atom emission spectrophotometer (ICP-AES) ICP-9000 (N + M, Thermo Jarrell-Ash Corp. I, USA) for metal elements (Ti and Zn) and Vario EL elemental analyzer (Elementar, Germany) for C and H elements.

2.4.9. Nitrogen sorption analysis. Nitrogen sorption measurements were performed on an ASAP 2020 (Micromeritics). The total surface area was calculated according to Brunauer, Emmett and Teller (BET) and the pore size distribution according to Barrett, Joyner and Halenda (BJH). The desorption branch was used for calculating the pore size distribution.

2.4.10. Diffuse reflectance spectra (DRS). Diffuse reflectance measurements were conducted on F7000 spectrophotometer through a synchronous scan mode. The powders were pressed into pellets, and $BaSO_4$ was used as a reference standard for correction of instrumental background. The reflectance was converted to absorbance by Kubelka–Munk function: $F(R) \propto \alpha/S = (1-R)^2/2R$,[7] where α is the absorption coefficient, S is the scattering coefficient, and R is the fractional diffuse reflectance.

3. Results and discussion

3.1 Synthesis and characterization of Zn_2Ti_3–GAH

In the synthesis of titanium complexes, $TiCl_4$ or titanium alkoxides, such as titanium tetrabutoxide (TTB) and titanium tetraisopropoxide (TTIP), were usually utilized as titanium source. However, owing to extreme moisture or water sensitivity, in most cases they underwent a fast and uncontrollable hydrolysis and oxolation process even at low temperature. Glycols could serve as a class of strong complexing reagents to greatly reduce the hydrolysis rates of a number of transition metal alkoxides/chlorides by forming glycolates or mixed alkoxide-glycolate derivatives.[4,5,10,40–42] With excess EG, herein some reactions such as eqn (1) and (2) occurred to yield titanium glycolate derivatives (*e.g.* $Ti(OCH_2CH_2O)(OCH_2CH_2OH)_2$ and $Ti(OCH_2CH_2O)_2(HOCH_2CH_2OH)$), which maintained a equilibrium in the solution.[5,10,42] The protons of chelated hydroxyl group of partially deprotonated EG ligands are more labile and reactive as a result of electron drift, and usually offer the functioning possibility towards alkoxides of other metals, yielding heterometallic glycolate alkoxides.[3–5,43,44]

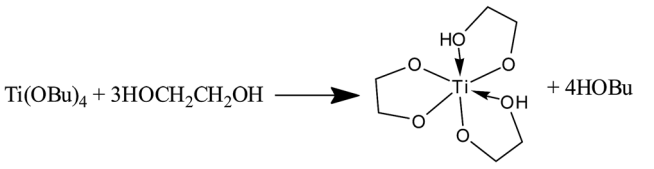

(1)

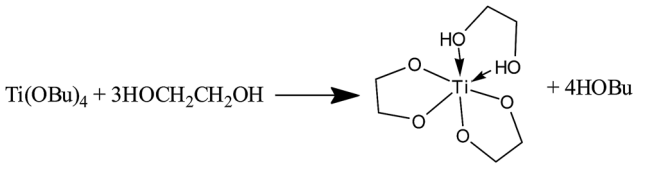

(2)

$Zn(CH_3COO)_2\cdot 2H_2O$ or anhydrous $Zn(CH_3COO)_2$ were found to produce crystalline Zn–EG–AC complex nanowires when refluxed in EG, which definitely comprised both EG species and acetate ions upon IR analysis.[45,46] Alcoholate groups were considered to be formed through the alcoholysis of acetate ions with alcohol due to its intrinsically weak basicity when dissolving some hydrated acetate salts in polyols medium.[47] Such a polyols (EG, glycerol, *etc.*) mediated process was employed to synthesize many other crystalline homometallic polyolate complexes (*e.g.* Sn(II), Pb(II), Co(II), Mn(II)) powders by reacting a metallic salt in appropriate polyalcohols instead of monoalcohols under heating.[47–49] Herein at room temperature and in EG $Zn(CH_3COO)_2\cdot 2H_2O$ was suggested to undergo pre-alcoholysis to de-coordinate acetic acid, producing zinc glycolate acetate species. They then interacted with titanium glycolate precursors to yield the Zn_2Ti_3–GAH, which precipitated from the reaction medium owing to low solubility.

Herein the Zn/Ti stoichiometric ratio (2 : 3) of Zn_2Ti_3–GAH is lower than that used in the starting materials (1 : 1), excess zinc acetate was left in the solution and discarded during the subsequent washing. Additionally, it was experimentally found that adopting the Zn/Ti molar ratio of 2 : 3 or 2 : 1 while keeping the constant concentration of titanium source displayed no effects on the chemical composition and crystal structure of the resulting Zn_2Ti_3–GAH. It means that controlled stoichiometric incorporation of Zn(II) and acetate ligand into the titanium glycolates is impossible. However, the morphology, precipitation process and production yield were affected. The appearance of milky colloids was delayed and the production yield was decreased at lower Zn/Ti ratio. With the stoichiometric ratio (2 : 3) of Zn/Ti, the first visible sign of the turbidity appeared in the clear solution ~1.5 h after the addition of zinc source while the yield was decreased to ~38% with respect to $[Ti(OC_4H_9)_4]$ supplied.

In the FT-IR spectrum of Zn_2Ti_3–GAH complex (see Fig. S1†) the strong and broad band associated with O–H stretching mode in the range of 3050–3500 cm^{-1} and the band at ~1665 cm^{-1} associated with the H–O–H bending mode evidenced the hydrate for Zn_2Ti_3–GAH complex. In a medium wavenumber range, the indicative absorption bands centered at ~1570 and 1420 cm^{-1} show that the acetate ligands (CH_3COO^-) were definitely involved in the Zn_2Ti_3–GAH complex. They were suggested to coordinate to the titanium atoms in a chelating coordination fashion given the relatively small difference between asymmetric and symmetric stretching vibrations ($\Delta\nu = \nu_a(COO^-) - \nu_s(COO^-) = 150\ cm^{-1}$).[17,50] In a lower wavenumber range, absorption bands centered at 1074 cm^{-1} (C–O stretching and C–O–H bending) and 885 and 914 cm^{-1} (CH_2 rocking vibration) were attributed to the modes of EG molecules and glycolate ligands. In the frequency range much lower than 700 cm^{-1}, the sharp absorption bands are assigned to stretching and bending vibrations of Ti–O bonds.[51]

The as-precipitated Zn_2Ti_3–GAH was highly crystalline (see Fig. S2†). However, such a XRD pattern cannot be indexed in the Inorganic Crystal Structure Database (ICSD) or International Centre for Diffraction Data (ICDD). A preliminary searching for peaks followed by analysis using McMasille program reveals a primitive monoclinic system (figures of merit M (20) = 64.85). The unit cell parameters were primarily determined to be a = 7.4564 Å, b = 9.4574 Å, c = 7.5544 Å, $\alpha = 90°$, $\beta = 120.093°$, $\gamma = 90°$, volume = 460.917 $Å^3$, which is extremely close to a hexagonal unit cell. The best space group estimated by Checkgroup is $P2_1/n$. No crystals suitable for single crystal X-ray diffraction analysis could be grown for Zn_2Ti_3–GAH. Presently it is beyond our ability to predict precisely the connectivity of glycolate and acetate ligands, and then to refine the molecule and crystal structures of Zn_2Ti_3–GAH. However, previous studies on the homometallic glycolates (Ti(IV), In(III), *etc.*) nanowires prepared by refluxing glycols and metal alkoxides or metal salts suggested that these complexes shared a chain-like structure.[41] Based on the similarities between our reaction and those reported in the literature, and the observation of a wire-like morphology, we believe that Zn_2Ti_3–GAH could also bear similar chains. A

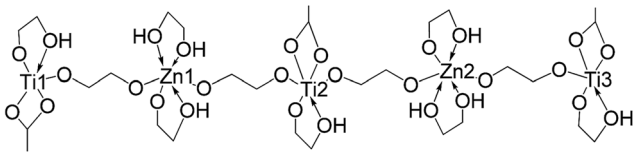

Scheme 1 Schematic representation of structural arrangement suggested for Zn_2Ti_3–GAH complex, where three titanium and two zinc atoms were alternately arranged in the chain and bridged by four totally deprotonated glycolate ligands (OCH_2CH_2O); each titanium atom was additionally chelated by one partially deprotonated glycolate ligand (OCH_2CH_2OH) and one acetate ligand (CH_3COO^-); each zinc atom was additionally chelated by one partially deprotonated glycolate ligand (OCH_2CH_2OH) and one neutral EG ($HOCH_2CH_2OH$) molecule; the neutral H_2O appeared as lattice water rather than coordinating water at metal atom, and was omitted for clarity; as a consequence, Ti1 and Ti3 are five-fold coordinated, while Ti2 is six-fold coordinated; both zinc atoms are six-fold coordinated.

schematic representation of suggested structural arrangement of Zn_2Ti_3–GAH complex was shown in Scheme 1.

SEM image of Zn_2Ti_3–GAH clearly shows that the crude particles (Fig. 1A) are mainly monodisperse microrods with the average diameter of ~0.5–1.5 μm and length of ~4.0–6.0 μm. Higher-magnification of TEM image on single microrod (Fig. 1B) depicts that it looks like micromesh with varying contrast (lower or higher) spanning the whole microrod. The presence of interior cavity implies that these microrods are of hierarchical structures assembled or stacked by smaller building blocks (~10–20 nm in size). Nitrogen sorption experiments (Fig. S3A†) showed a broad distribution of pore size from micropore to large pore, with sharp peaks at ~2.4 and 3.8 nm. The BET surface area was ~21.28 $m^2\ g^{-1}$. Contrary to power XRD analysis, high-resolution TEM (Fig. 1C) and SAED (see inset of Fig. 1B) on single microrod did not reveal the high

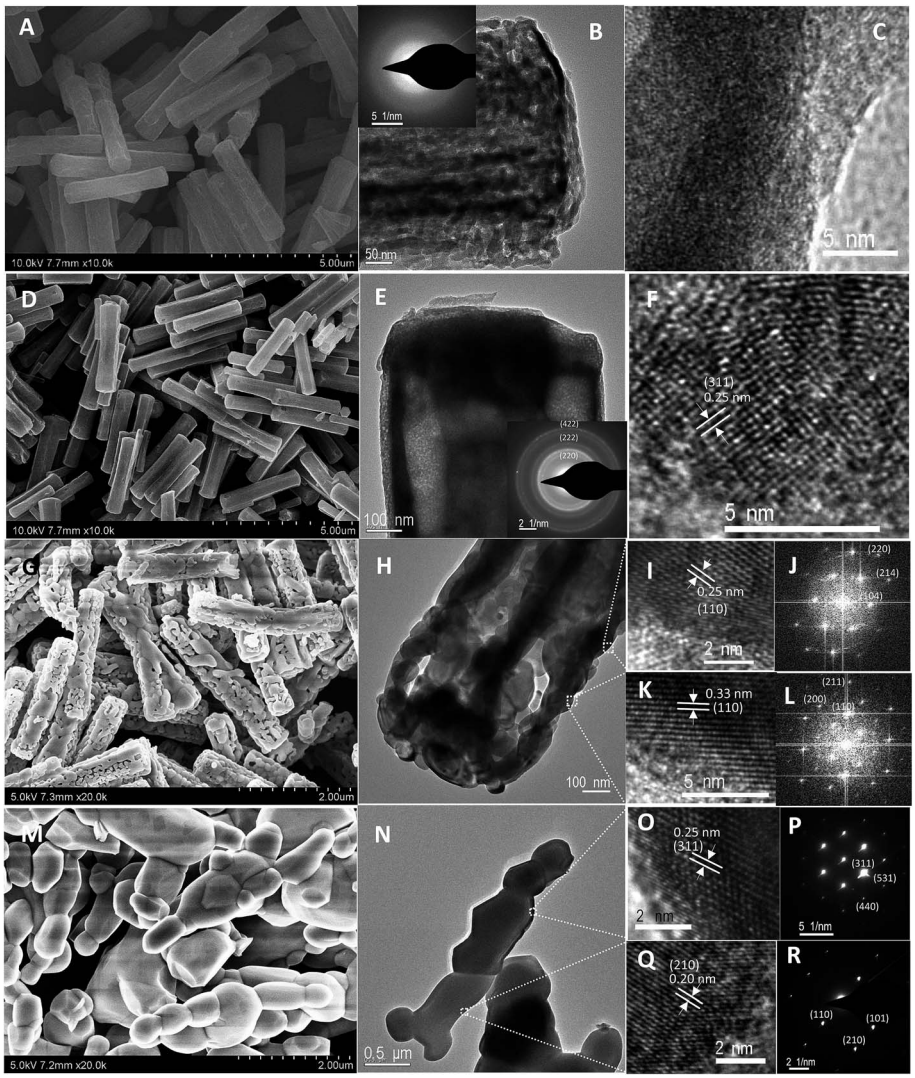

Fig. 1 SEM, TEM and HRTEM images, FFT as well as SAED patterns of zinc titanium glycolate acetate hydrate (Zn_2Ti_3–GAH) (A–C) and the products of zinc titanate *via* thermal treatment at 500 °C for 3 h ((D–F), $Zn_2Ti_3O_8$), 700 °C for 2 h ((G–L), r-TiO_2 supported h-$ZnTiO_3$) and 950 for 3 h ((M–R), r-TiO_2 supported Zn_2TiO_4). The insets of (B) and (E) are the SAED patterns taken on the single microrod, respectively; (I and K) are the HRTEM images acquired on the squared areas of microrod in (H); (J and L) are the FFT patterns of (I and K), respectively; (O and Q) are the HRTEM images acquired on the squared areas of adjacent grains in (N); (P and R) are the SAED patterns performed on the adjacent grains in (N). The *d* spacing and corresponding crystallographic planes were indicated in the HRTEM images.

crystallinity since no lattice fringes and diffraction rings or spots appeared under extensive observations. These are mostly likely due to the structural destruction by high-energy electron beam. The TEM-EDS analysis (Fig. S4†) revealed a Zn/Ti molar ratio near ~2 : 3, which agree well with the elemental analysis. In contrast, regular microrods were also observed at Zn/Ti ratio lower than 2 : 1, but many more irregular particles along with microrods appeared when adopting the Zn/Ti ratio lower than 1 : 1.

FT-IR spectrum of Zn_2Ti_3–GAH definitely indicates the presence of glycolate and acetate ligands, however, the solid-state CPMAS ^{13}C NMR spectrum of Zn_2Ti_3–GAH (see Fig. S5†) only displayed three resonance signals at $\delta \sim 70$ ppm for methylene [–OCH_2–] group (two stronger signals at δ 74.130, 61.295 ppm and one weak 63.910 ppm), no resonances around $\delta \sim 25$ (CH_3 region) and ~180 ppm (COO region) related to acetate groups were detected mostly likely due to its low content.[52] The signal at 74.130 ppm was assigned to chelated glycolate ligand, while the signal at 61.295 and 63.910 ppm were assigned to neutral glycols molecules.[44] In solution only one resonance of ^{13}C of free glycols was detected at ~63.249 ppm (Fig. S6F†). Herein crystallization of EG solvent in the microstructure of Zn_2Ti_3–GAH and then the interactions of coordination and hydrogen bonding, were considered to shield the principle resonance to ~61.295 ppm. In contrast, solution ^1H and ^{13}C NMR spectra (Fig. S6†) exhibit a number of peaks fallen in the region of methyl and methylene groups due to the dissociation of Zn_2Ti_3–GAH and/or further reactions in deuterated DMSO. Indeed, immersing Zn_2Ti_3–GAH in DMSO changed the crystallinity and morphology greatly (see Fig. S7B and S8C and D†). The materials became amorphous after soaking overnight; many separated small nanoparticles (~50 nm) were released along with the remaining microrods. The DMSO solvent damaged the Zn_2Ti_3–GAH mostly likely starting from the extraction of neutral molecules (EG and H_2O) in the microstructures.

Similar to many other crystalline homometallic glycolate powders,[40,41,47–49] the solubility of Zn_2Ti_3–GAH was also poor in common organic solvents, however, molecule ion peak of which in MS (see Fig. 2B) was detected by using DMF at *m/z* 1136.95 (theoretical 1137.06), corresponding to $[C_{28}H_{65}O_{29}Ti_3Zn_2]^+$, and the experimental isotopic pattern (Fig. 2C) matches exactly with

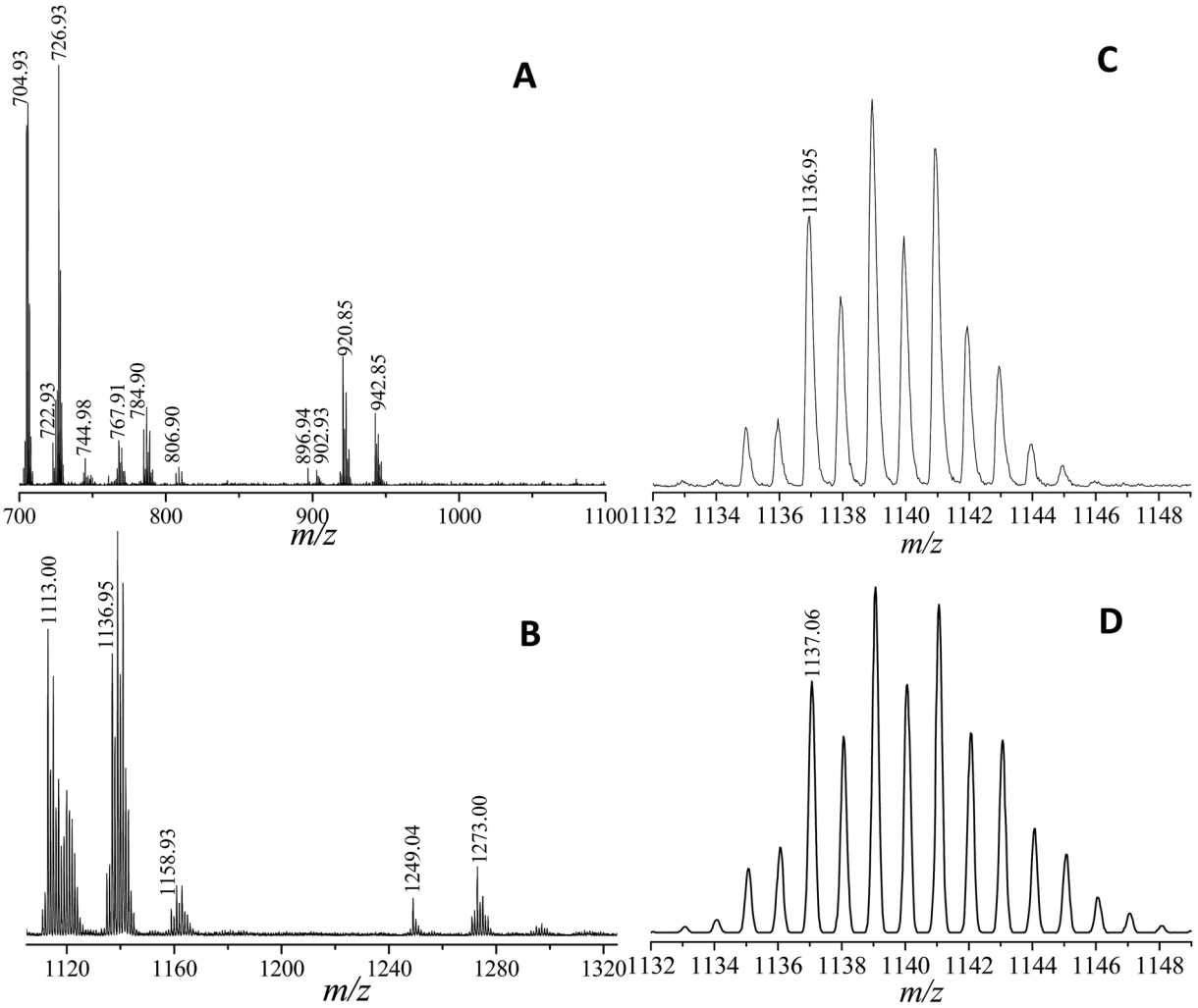

Fig. 2 (A and B) MS obtained after treating Zn_2Ti_3–GAH in DMF; (C and D) MS of Zn_2Ti_3–GAH; the experimentally obtained isotopic distribution pattern (C) for $[M + H]^+$ correlates well with the calculated pattern (D).

the simulated pattern (Fig. 2D). Considering the outstanding high stability of titanium glycolate toward moisture,[10,42] the present as-synthesized complex was suggested to contain no oxo ligands inside. In addition, given the starting materials and solvent used, molecular ligands determined by FTIR, thermal evolution by TG-DTA discussed below as well as charge balance held in the molecular formula, Zn_2Ti_3–GAH was thus tentatively formulated as $Zn_2Ti_3(OCH_2CH_2O)_4(OCH_2CH_2OH)_5(CH_3COO)_3 \cdot 2HOCH_2CH_2OH \cdot H_2O$. Additionally, MS also shows several molecule ion peaks of other species (see Fig. 2A and B and S9†). It was considered that a small amount of Zn_2Ti_3–GAH was destroyed and/or dissociated into many other complexes of lower nuclearities when dispersed in solvents for MS analysis. Similar to the case of DMSO, soaking Zn_2Ti_3–GAH in DMF overnight also changed the crystallinity and morphology but proceeded slowly. After one time soaking the diffraction peak intensity was dramatically reduced (Fig. S7C†), and then the materials became completely amorphous without any diffraction peaks after second immersion (Fig. S7D†); the surface of microrods became scraggly with a small amount of ~50 nm nanoparticles (see Fig. S8E–H†). Additionally, after immersing Zn_2Ti_3–GAH in H_2O overnight, as shown in Fig. S7E and S8I and J,† the materials also became amorphous; many microrods were retained but with cavities inside, some microrods were broken into smaller pieces. It is apparent that solvents destroyed the Zn_2Ti_3–GAH in different ways.

The thermal properties of Zn_2Ti_3–GAH were also examined by TG-DTA in air. As shown in Fig. 3, S10 and S11,† thermal behaviors could be mainly divided into four steps, namely, initial endothermic stage, subsequent two exothermic combustion steps, and a last exothermic process. Each process, especially the initial endothermic stage and subsequent combustions, resulted in a great mass loss. The total weight loss was ~66.6% when heated to 1000 °C. The endothermic peak at ~180 °C associated with a ~39.0% mass loss was in agreement with the theoretical loss upon considering the departure of surface moisture, hydration water, lattice EG molecules and partially deprotonated glycolate groups (–OCH_2CH_2OH). EG is known to be a relatively stable organic compound with a boiling point of 197.6 °C.[53] The intercalation of molecule EG therefore stabilizes the compound up to ~180 °C. The first exotherm was associated with the combustion of totally deprotonated glycolate ligands [$(OCH_2CH_2O)_4$], with a mass loss of ~10.6% well comparable with the calculated value. The second sharp exotherm was attributed to the combustion of acetate ligand, with a weight loss (~13.1%) slightly lower than the calculated value (~15.5%) due to the progressive release. The last weaker exothermic process continued in a broad temperature range was related to the slow burnout of the organic residuals and crystallization behaviors of zinc titanate.

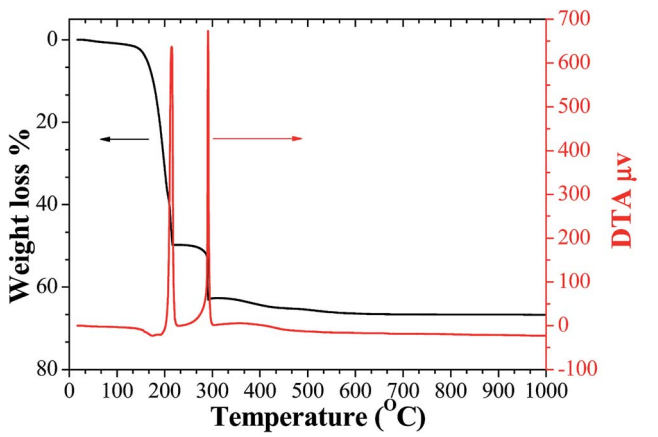

Fig. 3 TG-DTA curves of zinc titanium glycolate acetate hydrate (Zn_2Ti_3–GAH).

TG-FTIR was used to examine the gas species evolved during heating of Zn_2Ti_3–GAH. Fig. 4 displays a two-dimensional (2D) wavenumber *versus* temperature FTIR spectrum. At temperature below ~52 °C, no vibration absorption could be detected, then some apparent absorption bands related to hydroxyl (O–H, 3650 cm^{-1}), methylene (CH_2, 2945, 2886 cm^{-1}), carbonyl (C=O, 1731 cm^{-1}) and C–O groups (1051 cm^{-1}) appeared, indicating the release of water, EG molecules and even some acetic species. In accordance with the endotherm in DTA, these bands became relatively stronger at ~200 °C. The C–H and C–O modes were still detected during the first exotherm (~210 °C) and but disappeared in the second one (~305 °C). It means that glycolate species underwent insufficient combustion into H_2O and CO_2 during the first exotherm and were completely removed from the solid structure below ~305 °C. The CO_2 modes in the range of 2265–2400 cm^{-1} started to appear after ~170 °C and nearly disappeared after the second combustion (~400 °C). They were mainly associated with the oxidation process and accordingly displayed stronger absorptions during the combustion processes. The absorption band of carboxyl ligand retained up to 700 °C, also indicating the slow release of acetate species. These carbonyl containing species are most likely to be acetic acid, acetone, or acetic anhydride according to previous studies on $Zn_5(OH)_8(CH_3CO_2)_2 \cdot nH_2O$.[52]

In a typical synthesis, milky colloids appeared ~1 h after the addition of zinc acetate solution. The growth of microrods in solution was studied by sampling at different periods of reaction time. As shown in Fig. S12A,† initially these colloids were mainly gel-like particles in morphology, which became less as the reaction proceeded. Rod-like particles appeared even after ~1.5 h and dominated the products rapidly. The nucleation and growth proceeded continuously; some microrods grew preferentially into a relatively large size in a short time. As shown in Fig. S12B,† the dimension of the some rods reached a diameter of 0.4 μm and a length of 2.0 μm in ~0.5 h. This was almost a limit of size in the following ~3 h (see Fig. S12C–G).† Moreover, during growth process many microrods were characterized by ill-shape, rough side and end faces. It was therefore believed that the growth of microrods followed an aggregation/packing process of the as-grown small particles. They collided and then coalesced and/or self-assembled into microrods for surface energy minimization according to the chemical bonding theory of single crystal growth.[54] In the reaction system, both polar solvent of EG and Zn_2Ti_3–GAH feature rich hydroxyl groups, which allow a variety of intermolecular forces such as hydrogen bonding and dipole–dipole electrostatic interaction, to promote

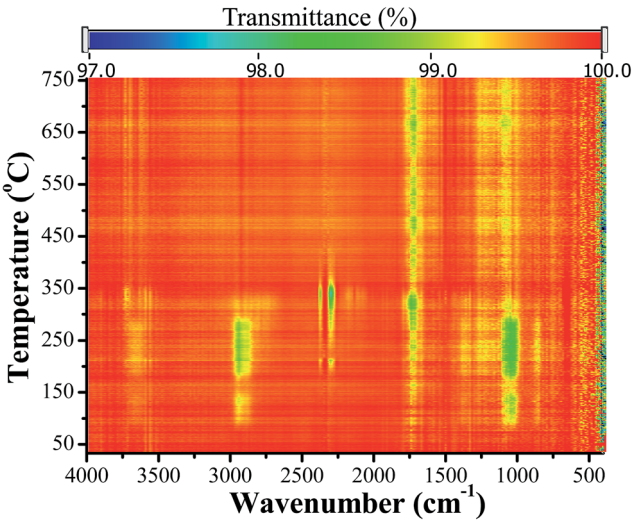

Fig. 4 A two-dimensional (2D) wavenumber *versus* temperature FTIR spectrum of gas species evolved during heating of Zn_2Ti_3–GAH; the rainbow colors indicate transmittance of the FTIR spectrum acquired at different temperature.

the self-assembly into more dynamic and complex structures.[55] In the following experiments, aging allowed for growing into much larger size, more regular shape and smoother surface *via* Oswald ripening.

3.2 Thermal evolution

Fig. 5 exhibits the XRD patterns of the thermally treated products of Zn_2Ti_3–GAH. It was found that crystallization and phase transition were dependent on the reaction temperature and time. After calcination at 500 °C for 2 h, the powder was weakly crystalline to X-ray diffraction, but it definitely crystallized into one phase with several well-defined broad peaks upon prolonged heating to 3 h. One set of sharp peaks appeared and overlapped the broad peaks when calcined at 600 °C for 2 h.

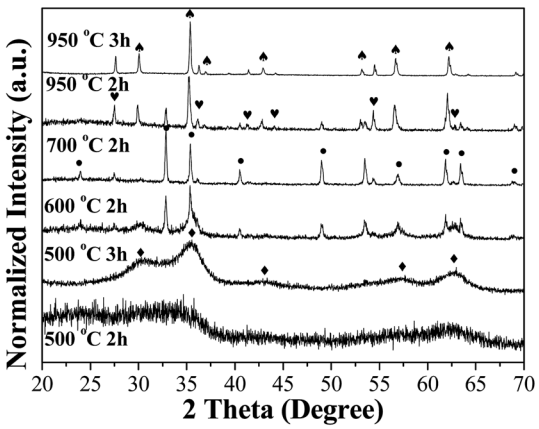

Fig. 5 XRD patterns of the zinc titanate obtained through calcinations of zinc titanium glycolate acetate hydrate (Zn_2Ti_3–GAH) at various temperatures for different times; each pattern was normalized to its maximum (◆ $Zn_2Ti_3O_8$; ● h-$ZnTiO_3$; ♠ Zn_2TiO_4; ♥ r-TiO_2).

These sharp peaks could be exclusively indexed to the hexagonal $ZnTiO_3$ (h-$ZnTiO_3$, ICDD File no. 14-0033).[24,25,56] Referring to the positions of these broad diffraction peaks, two possible assignments to c-$ZnTiO_3$ (ICDD File no. 39-0190, 1 : 1 of Ti/Zn ratio) or to cubic $Zn_2Ti_3O_8$ (ICDD File no. 87-1781, 3 : 2 of Ti/Zn ratio), are available due to the nearly same reflection positions.[24,51,57] A complete transition to h-$ZnTiO_3$ occurred upon increasing the calcinations temperature to 700 °C. However, single phase of h-$ZnTiO_3$ was not accordingly yielded; a byproduct of rutile TiO_2 (r-TiO_2, ICDD File no. 21-1276) appeared. Titania is well known to exist in three naturally occurring polymorphic forms, namely crystalline phases of anatase (a-TiO_2), rutile and brookite. r-TiO_2 represents the thermodynamically stable form at higher temperature and a-TiO_2 shows higher kinetic stability. The production of r-TiO_2 upon continuous calcination of the amorphous precursors usually follows the first crystallization of a-TiO_2 phase at low temperature (~500 °C) and then a phase transition (~650 °C).[40] However, herein the a-TiO_2 was not yet observed when conducting the calcination in 500–700 °C range. It is considered that the production of r-TiO_2 was not from any separated amorphous complexes precursors co-precipitated with Zn_2Ti_3–GAH but from the direct decomposition of the crystalline material obtained by calcining Zn_2Ti_3–GAH complex at 500 °C for 3 h. Thereby, the above undetermined crystalline phase must possess a Ti/Zn stoichiometric ratio higher than 1 : 1; it is exclusively determined to be cubic phase of $Zn_2Ti_3O_8$ rather than c-$ZnTiO_3$. This is in accord with previous reports that the $Zn_2Ti_3O_8$ directly decomposed into r-TiO_2 and h-$ZnTiO_3$ upon calcination.[57,58] Note that the present $Zn_2Ti_3O_8$ obtained was only thermodynamically stable at ~500 °C, while it was reported earlier that $Zn_2Ti_3O_8$ could be stable until ~650, 800 and 820 °C without decomposition.[51,57,58] Heating at higher temperature of 950 °C enabled the h-$ZnTiO_3$ further decompose into the Zn_2TiO_4 (cubic system, ICDD File no. 25-1164) and r-TiO_2. Such a structural transition was completed at the same calcination temperature but for 3 h. Overall, a schematic illustration of phase transformation of Zn_2Ti_3–GAH under calcination was shown in Scheme 2.

As shown in Fig. 1, although the compositions as well as the structures of these zinc titanate are very different from the as-synthesized product, both of them held the shape of the Zn_2Ti_3–GAH until ~700 °C. After calcination at 500 °C the diameter of microrods shrank to 0.5–1.0 μm, length to 2.0–3.0 μm (see Fig. 1D) due to the removal of organic moieties. TEM image of single microrod in Fig. 1E shows that the microrods are still porous but with a slightly larger pore size among the

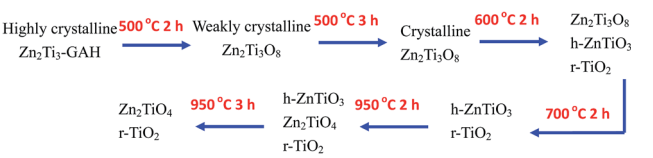

Scheme 2 Schematic illustrations of phase transformation process of Zn_2Ti_3–GAH under calcination.

packed nanoparticles. The pore size distribution by BJH method upon nitrogen sorption analysis (Fig. S3B†) shows a sharp peak at ~3.4 nm with a long tail in the regions of mesopore and large pore structures while the BET surface area increased to 34.28 $m^2 g^{-1}$ due to the removal of organic species. The SAED pattern (see the inset of Fig. 1E) on the microrod comprised some diffraction rings, indicating the polycrystallinity. These rings could be indexed to different crystal planes of single phase of cubic $Zn_2Ti_3O_8$. High resolution TEM image (see Fig. 1F) exhibits some lattice fringes of the nanounits (~5–10 nm) assembled in the microrods. The observed *d*-spacing of ~0.25 nm is in good agreement with the lattice spacing of the (311) plane of cubic $Zn_2Ti_3O_8$. At elevated temperature of 700 °C the resulting sample retained the rod shape, but the packed nanouints further grew into ~100–400 nm in size and left much larger cavity in the microrods (see Fig. 1G and H). The pore size also shows a broad distribution from micropore to large pore with peaks at 1.7 and 30.1 nm upon N_2 adsorption–desorption analysis (Fig. S3C†) while the BET surface area was dramatically decreased to 5.29 $m^2 g^{-1}$. In accordance with the XRD analysis that two phases of the h-$ZnTiO_3$ and r-TiO_2 were yielded under calcinations; herein it means that both phases occurred with each other in the microrod precursor, which could thus be termed as r-TiO_2 supported h-$ZnTiO_3$. Both h-$ZnTiO_3$ (see Fig. 1I) and r-TiO_2 nanoparticles (see Fig. 1K) were highly crystalline and imaged by high resolution TEM in single microrod where the interplanar spacing and corresponding crystal planes were indicated. Their FFT patterns (see Fig. 1J and L) characterized by regularly arranged spots indicate the single crystallinity. It is believed that a heterojunction of r-TiO_2–h-$ZnTiO_3$ formed in the particles-packed microrods. As shown in Fig. 1M and N, the Zn_2TiO_4 yielded upon thermal treatment at 950 °C did not retain the rod morphology, many bigger particles ~0.4–1.0 μm in size were observed; some of them were grown into a chain. The porosity property accordingly disappeared. No typical isotherms with hysteresis loops were observed in nitrogen sorption experiment (Fig. S3D†). The BET surface area was only 0.02 $m^2 g^{-1}$. High resolution TEM on adjacent grains indicates the intergrowth of Zn_2TiO_4 (Fig. 1O) and r-TiO_2 (Fig. 1Q) grains in one chain, forming a heterojunction structure (named as r-TiO_2 supported Zn_2TiO_4). They are both of single crystallinity confirmed by SAED (Fig. 1P for Zn_2TiO_4; Fig. 1R for r-TiO_2). The formation of r-TiO_2 supported titanate obtained by post-treatment at elevated temperature was analogue to previous report on TiO_2 supported $Ce_2Ti_2O_7$.[15]

To date, a variety of routes have been developed to prepare zinc titanate ($Zn_xTi_yO_z$) in the form of bulk solid ceramics, nano/microcrystalline powders, thin films, such as solid state reaction method,[31,32,56] sol–gel processing,[24–30] metallo-organic deposition (MOD) technique,[38] radio frequency magnetron reactive sputtering.[59] However, only a few studies have reported on the shape and size-controlled synthesis. Zinc titanate fibers were prepared by electrospinning.[60] $Zn_2Ti_3O_8$ nanowires were obtained *via* an ion-exchange reaction between the Na_xH_{2-x}-Ti_3O_7 nanotubes and a Zn^{2+} contained ammonia solution.[58] Twinned Zn_2TiO_4 nanowires were synthesized using ZnO nanowires as a template or by an ordered assembly of nanobricks, respectively.[61,62] One SSP route to zinc titanate films through sol–gel processing of Zn–Ti–POBC bimetallic complex was previously reported.[20] The temperature-dependent structure evolution of $ZnTiO_3$ by small angle X-ray scattering (SAXS) illustrated the advantage of SSP route to avoid the phase separation into regions with different compositions on the nanoscale level in the gel stage, compared to materials prepared from two individual precursors.[20] In contrast, the SSP route presented herein benefits over the shape preservation of the precursors and *in situ* intergrowth of different phases (*i.e.* heterostructures) under suitable calcinations due to the confinement in the specific microrod domains.

3.3 Optical absorption and band gaps

The UV-visible Kubelka–Munk corrected diffuse reflectance spectra of Zn_2Ti_3–GAH, $Zn_2Ti_3O_8$, r-TiO_2 supported h-$ZnTiO_3$ and r-TiO_2 supported Zn_2TiO_4 are shown in Fig. 6 at their absorption edges. These are associated with the O → Ti and O → Zn charge transfer transitions, from which the band gap can be determined.[15] In agreement with the single phase characteristic, Zn_2Ti_3–GAH and $Zn_2Ti_3O_8$ both show a steep absorption edge while r-TiO_2 supported h-$ZnTiO_3$ and r-TiO_2 supported Zn_2TiO_4 exhibit step-like edge due to the phase separation. The band gap was estimated *directly* by extrapolation of the absorption edge data to the energy axis (Fig. S13†). Zn_2Ti_3–GAH and $Zn_2Ti_3O_8$ show the band gaps of 3.84 and 3.66 eV, respectively. The nature of electronic transitions were checked by fitting the absorption edges to the well-known "$\alpha = B(h\nu - E_g)^n/h\nu$" equation, where α is the linear absorption coefficient ($F(R)$, the Kubelka–Munk function, for an infinitely thick material), B is a proportionality constant, $h\nu$ (in eV) is the photon energy at each point of the scan and E_g (in eV) is the energy of band gap.[7] An excellent fit was got for the exponent

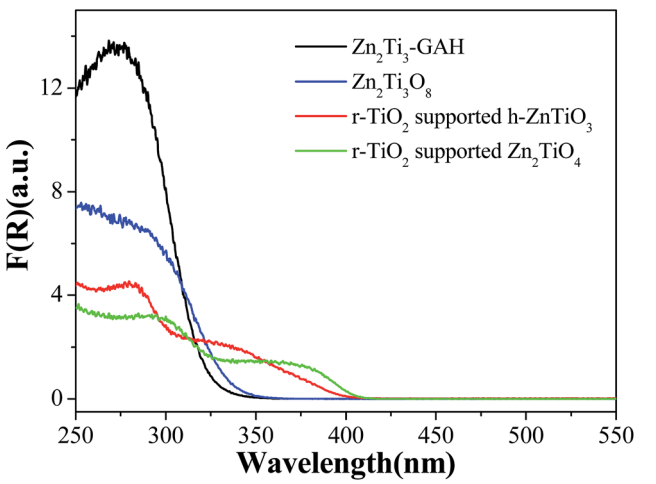

Fig. 6 Diffuse reflectance spectra of Zn_2Ti_3–GAH, $Zn_2Ti_3O_8$ (*via* thermal treatment of Zn_2Ti_3–GAH at 500 °C for 3 h), r-TiO_2 supported h-$ZnTiO_3$ (*via* thermal treatment of Zn_2Ti_3–GAH at 700 °C for 2 h) and r-TiO_2 supported Zn_2TiO_4 (*via* thermal treatment of Zn_2Ti_3–GAH at 950 °C for 3 h) at the absorption edges. $F(R)$ is the Kubelka–Munk function.

$n = 2$ and none at all for $n = 0.5$, which suggests that both Zn_2Ti_3–GAH and $Zn_2Ti_3O_8$ feature allowed indirect band gap transition. Using the same extrapolation method, two band gap values of 3.08 and 3.75 eV were determined for r-TiO_2 supported h-$ZnTiO_3$, and 3.03 and 3.54 eV for r-TiO_2 supported Zn_2TiO_4. The band gap of around 3.0 eV coincides with the value reported for rutile phase and thus,[7] h-$ZnTiO_3$ and Zn_2TiO_4 have the band gap of 3.75 and 3.54 eV, respectively, which are comparable to previous reports.[59,63] Additionally, it can be clearly seen in Fig. 6 that the sample of r-TiO_2 supported Zn_2TiO_4 has much stronger r-TiO_2 related absorption than that in r-TiO_2 supported h-$ZnTiO_3$. Indeed, the former has a much higher content of r-TiO_2 than the latter due to further thermal decomposition of h-$ZnTiO_3$ at elevated temperature.

3.4 Photocatalytic properties

The photocatalytic activities of Zn_2Ti_3–GAH, $Zn_2Ti_3O_8$, r-TiO_2 supported h-$ZnTiO_3$ and r-TiO_2 supported Zn_2TiO_4 were evaluated at room temperature through the photodegradation of the dye MB aqueous solution under UV irradiation, as shown in Fig. 7. The Zn_2Ti_3–GAH showed no UV photoactivity with similar self-degradation to homogeneous MB. In contrast, all of the thermally treated products exhibited enhanced activity. The heterostructures contained samples had much higher activity. Particularly, r-TiO_2 supported h-$ZnTiO_3$ even bearing smaller specific surface area than the sample of $Zn_2Ti_3O_8$ and lower content of r-TiO_2 than r-TiO_2 supported Zn_2TiO_4 was but more photoactive, and nearly degraded all of the given MB in 20 min, which was comparable to the commercially available Degussa P25 TiO_2. Titania generally shows higher photocatalytic activity; however, herein the higher content of r-TiO_2 in the sample of r-TiO_2 supported Zn_2TiO_4 did not accordingly exhibit enhanced photocatalysis. This implies that h-$ZnTiO_3$ is a more efficient UV catalyst than both $Zn_2Ti_3O_8$ and Zn_2TiO_4, or most probably the occurring heterojunction of r-TiO_2–h-$ZnTiO_3$ benefits over the effective separation of photogenerated charge carriers of electron–hole pairs, which would migrate to the surface of materials and initiate the catalytic reaction with surface adsorbed materials. As shown in Fig. 7B, the fitting of the initial $\ln(C/C_0)$ *versus* time data to the pseudo-first order rate law gave the apparent rate constant K in each photodegradation reaction. The value of r-TiO_2 supported h-$ZnTiO_3$ was ~27.3% of commercially available Degussa P25 TiO_2.

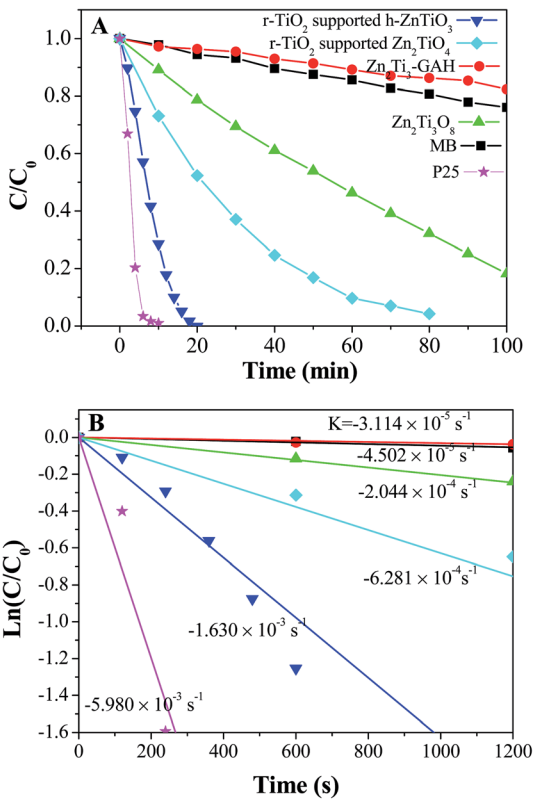

Fig. 7 (A) Methylene blue (MB) photodegradation by C/C_0 as a function of the reaction time under ~29.2 mW cm^{-2} UV irradiation of a Hg lamp and (B) fitting plots of initial $\ln(C/C_0)$ *versus* time data to the pseudo-first order reaction rate law ($\ln(C/C_0) = -Kt$), where K is the rate constant (s^{-1}), C_0 is the initial concentration of MB after the equilibrium absorption, and C is the concentration of MB at time t: (■) MB solution without catalyst, (★) using Degussa P25 TiO_2 as the photocatalyst, (●) using Zn_2Ti_3–GAH as the photocatalyst, (▲) using $Zn_2Ti_3O_8$ as the photocatalyst, (▼) using r-TiO_2 supported h-$ZnTiO_3$ as the photocatalyst and (♦) using r-TiO_2 supported Zn_2TiO_4 as the photocatalyst.

4. Conclusions

In summary, we facilely synthesized one new heterobimetallic complex of zinc titanium glycolate acetate hydrate by room-temperature homogeneous precipitation *via* the reaction of titanium glycolate precursors with zinc glycolate acetate species in EG ($HOCH_2CH_2OH$) solution and tentatively denoted it as $Zn_2Ti_3(OCH_2CH_2O)_4(OCH_2CH_2OH)_5(CH_3COO)_3 \cdot 2HOCH_2CH_2OH \cdot H_2O$ on the basis of extensive characterizations on chemical composition, crystal structure, morphology, growth mechanism and thermal behaviors. The obtained Zn_2Ti_3–GAH was of highly crystalline monoclinic phase and porous microrod morphology. Thermal decomposition of SSP of Zn_2Ti_3–GAH produced different phases of zinc titanate with the rod-like morphology preserved up to ~700 °C. Cubic phase of $Zn_2Ti_3O_8$ was obtained by calcining at 500 °C, while rutile TiO_2 (r-TiO_2) supported hexagonal phase of $ZnTiO_3$ (h-$ZnTiO_3$) were produced at 700 °C. The r-TiO_2 supported Zn_2TiO_4 were further yielded in the form of dispersed particles or chains at higher temperature (950 °C 3 h). Benefiting from the SSP route and the confinement of specific microrod domains of Zn_2Ti_3–GAH precursors, some heterostructures of r-TiO_2–$ZnTiO_3$ and r-TiO_2–Zn_2TiO_4 were formed during the programmable calcination. The photocatalysis against degradation of MB indicated that the thermally treated products of zinc titanate possessed enhanced activity. Specially, r-TiO_2 supported h-$ZnTiO_3$ displayed the reaction rate constant of 0.00163 s^{-1}, which was comparable with that of commercially available Degussa P25 TiO_2. This probably related to the more effective charge separation in the r-TiO_2–$ZnTiO_3$ heterostructure assembled in the microrods.

Acknowledgements

G.-H. P is grateful to the New Energy and Industrial Technology Development Organization (NEDO) of Japan for financial support. This work is also financially supported by the National Natural Science Foundation of China (Grant no. 51172226, 61275055, 51202019, 11274007, 11174278 and 51402284), Twelfth Five-Year Plan of The Education Department of Jilin Province for Science and Technology Study (Grant no. 2014-266) and the Natural Science Foundation of Jilin province (201205024, 20140101169JC and 20150520022JH). G.-H. P thanks Prof. Qing Wang and Dr Ming-Shu Chi in Northeast Dianli University for the measurement of TG-FTIR spectra. G.-H. P also acknowledges Prof. Zaicheng Sun and Dr Guoqiang Zhang in Changchun Institute of Optics, Fine Mechanics and Physics Chinese Academy of Sciences for the assistance of measurements of photocatalytic activities. G.-H. P is grateful to Dr Zijiang Jiang and Dr Yihan Zhou in Changchun Institute of Applied Chemistry Chinese Academy of Sciences for many stimulating scientific discussions on NMR and MS, respectively.

References

1 R. C. Mehrotra, A. Singh and S. Sogani, *Chem. Rev.*, 1994, **94**, 1643–1660.
2 R. C. Mehrotra and A. Singh, *Polyhedron*, 1998, **17**, 689–694.
3 L. G. Hubert-Pfalzgraf, *Coord. Chem. Rev.*, 1998, **178–180**, 967–997.
4 A. Singh and R. C. Mehrotra, *Coordin. Chem. Rev.*, 2004, **248**, 101–118.
5 D. C. Bradley, R. C. Mehrotra, I. P. Rothwell and A. Singh, *Alkoxo, and Aryloxo Derivatives of Metals*, Elsevier, 2001.
6 L. Rozes and C. Sanchez, *Chem. Soc. Rev.*, 2011, **40**, 1006–1030.
7 P. Coppens, Y. Chen and E. Trzop, *Chem. Rev.*, 2014, **114**, 9645–9661.
8 P. D. Matthews, T. C. King and D. S. Wright, *Chem. Commun.*, 2014, **50**, 12815–12823.
9 Ł. John and P. Sobota, *Acc. Chem. Res.*, 2014, **47**, 470–481.
10 D. Wang, R. Yu, N. Kumada and N. Kinomura, *Chem. Mater.*, 1999, **11**, 2008–2012.
11 G. A. Seisenbaeva, T. Mallah and V. G. Kessler, *Dalton Trans.*, 2010, **39**, 7774–7779.
12 S. Eslava, M. McPartlin, R. I. Thomson, J. M. Rawson and D. S. Wright, *Inorg. Chem.*, 2010, **49**, 11532–11540.
13 S. Eslava, F. Hengesbach, M. McPartlin and D. S. Wright, *Chem. Commun.*, 2010, **46**, 4701–4703.
14 S. Eslava, B. P. R. Goodwill, M. McPartlin and D. S. Wright, *Inorg. Chem.*, 2011, **50**, 5655–5662.
15 Y. Lv, M. Yao, J. P. Holgado, T. Roth, A. Steiner, L. Gan, R. M. Lambert and D. S. Wright, *RSC Adv.*, 2013, **3**, 13659–13662.
16 Y.-H. Lai, T. C. King, D. S. Wright and E. Reisner, *Chem.–Eur. J.*, 2013, **19**, 12943–12947.
17 C. Artner, A. Koyun, M. Czakler and U. Schubert, *Eur. J. Inorg. Chem.*, 2014, 5008–5014.
18 C. Artner, S. Kronister, M. Czakler and U. Schubert, *Eur. J. Inorg. Chem.*, 2014, 5596–5602.
19 M. Hamid, A. A. Tahir, M. Mazhar, M. Zeller and A. D. Hunter, *Inorg. Chem.*, 2007, **46**, 4120–4127.
20 J. Yang, J. Akbarzadeh, C. Maurer, H. Peterlik and U. Schubert, *J. Mater. Chem.*, 2012, **22**, 24034–24041.
21 Y. Qu, W. Zhou, Z. Ren, S. Du, X. Meng, G. Tian, K. Pan, G. Wang and H. Fu, *J. Mater. Chem.*, 2012, **22**, 16471–16476.
22 Y. Qu, W. Zhou, Z. Ren, G. Wang, B. Jiang and H. Fu, *ChemCatChem*, 2014, **6**, 2258–2262.
23 Y. Qu, W. Zhou and H. Fu, *ChemCatChem*, 2014, **6**, 265–270.
24 J. Mrázek, L. Spanhel, G. Chadeyron and V. Matějec, *J. Phys. Chem. C*, 2010, **114**, 2843–2852.
25 G. Starukh, S. Toscani, S. Boursicot and L. Spanhel, *Z. Phys. Chem.*, 2007, **221**, 349–360.
26 E. Hosono, S. Fujihara, M. Onuki and T. Kimura, *J. Am. Ceram. Soc.*, 2004, **87**, 1785–1788.
27 L. Wang, H. Kang, D. Xue and C. Liu, *J. Cryst. Growth*, 2009, **311**, 611–614.
28 H. T. Kim, Y. Kim, M. Valant and D. Suvorov, *J. Am. Ceram. Soc.*, 2001, **84**, 1081–1086.
29 M. Zheng, R. Yu, J. Chen, J. Zhao, G. Liu, X. Xing and J. Meng, *J. Am. Ceram. Soc.*, 2008, **91**, 544–547.
30 Y. Chang, Y. Chang, I. Chen, G. Chen and Y. Chai, *J. Cryst. Growth*, 2002, **243**, 319–326.
31 H. T. Kim, S. Nahm and J. D. Byun, *J. Am. Ceram. Soc.*, 1999, **82**, 3476–3480.
32 H. Obayashi, Y. Sakurai and T. Gejo, *J. Solid State Chem.*, 1976, **17**, 299–303.
33 V. B. Reddy, S. P. Goel and P. N. Mehrotar, *Mater. Chem. Phys.*, 1984, **10**, 365–373.
34 S. Wang, M. Lu, F. Gu, C. Song, D. Xu, D. Yuan, G. Zhou and Y. Qi, *Inorg. Chem. Commun.*, 2003, **6**, 185–188.
35 S. Wang, F. Gu, M. Lu, W. Zou, S. Liu, D. Xu, D. Yuan, G. Zhou and Y. Qi, *J. Phys. Chem. Solids*, 2004, **65**, 1243–1245.
36 S. F. Wang, F. Gu, M. K. Lu, C. F. Song, D. Xu, D. R. Yuan and S. W. Liu, *Chem. Phys. Lett.*, 2003, **373**, 223–227.
37 M. Pineda, J. L. G. Fierro, J. M. Palaciosa, C. Cilleruelo, E. García and J. Ibarra, *Appl. Surf. Sci.*, 1997, **119**, 1–10.
38 Z. X. Chen, A. Derking, W. Koot and M. P. Dijk, *J. Catal.*, 1996, **161**, 730–741.
39 Z. Hong, M. Wei, Q. Deng, X. Ding, L. Jiang and K. Wei, *Chem. Commun.*, 2010, **46**, 740–742.
40 O. Yamamoto, T. Sasamoto and M. Inagaki, *J. Mater. Res.*, 1992, **7**, 2488–2491.
41 X. Jiang, Y. Wang, T. Herricks and Y. Xia, *J. Mater. Chem.*, 2004, **14**, 695–703.
42 X. Jiang, T. Herricks and Y. Xia, *Adv. Mater.*, 2003, **15**, 1205–1209.
43 R. C. Mehrotra, A. Singh, M. Bhagat and J. Godhwani, *J. Sol-Gel Sci. Technol.*, 1998, **13**, 45–49.
44 G. J. Gainsford, T. Kemmitt, C. Lensink and N. B. Milestone, *Inorg. Chem.*, 1995, **34**, 746–748.
45 J. W. Zhang, P. L. Zhu, Z. W. Li, J. M. Chen, Z. S. Wu and Z. J. Zhang, *Nanotechnology*, 2008, **19**, 165605.
46 C. Tian, W. Li, Q. Zhang, K. Pan and H. Fu, *Mater. Res. Bull.*, 2011, **46**, 1283–1289.

47 D. Larcher, G. Sudant, R. Patrice and J.-M. Tarascon, *Chem. Mater.*, 2003, **15**, 3543–3551.
48 E. W. Radoslovich, M. Raupach, P. G. Slade and R. M. Taylor, *Aust. J. Chem.*, 1970, **23**, 1963–1971.
49 A. M. Cao, J. S. Hu, H. P. Liang and L. J. Wan, *Angew. Chem., Int. Ed.*, 2005, **44**, 4391–4395.
50 A. Moezzi, M. B. Cortie, R. Shimmon and A. M. McDonagh, *Eur. J. Inorg. Chem.*, 2013, 5133–5137.
51 O. Yamaguchi, M. Morimi, H. Kawabata and K. Shimizu, *J. Am. Ceram. Soc.*, 1987, **70**, C97–C98.
52 A. Moezzi, A. McDonagh, A. Dowd and M. Cortie, *Inorg. Chem.*, 2013, **52**, 95–102.
53 A. Kasai and S. Fujihara, *Inorg. Chem.*, 2006, **45**, 415–418.
54 C. Sun and D. Xue, *CrystEngComm*, 2014, **16**, 2129–2135.
55 G. Ma, Y. Zhou, X. Li, K. Sun, S. Liu, J. Hu and N. A. Kotov, *ACS Nano*, 2013, **7**, 9010–9018.
56 F. H. Dulin and D. E. Rase, *J. Am. Ceram. Soc.*, 1960, **43**, 125–131.
57 J. Yang and J. H. Swisher, *Mater. Charact.*, 1996, **37**, 153–159.
58 Z. Hong, M. Wei, Q. Deng, X. Ding, L. Jiang and K. Wei, *Chem. Commun.*, 2010, **46**, 740–742.
59 C. Ye, S. S. Pan, X. M. Teng, H. T. Fan and G. H. Li, *Appl. Phys. A: Mater. Sci. Process.*, 2008, **90**, 375–378.
60 Z. Cai, J. Li and Y. Wang, *J. Alloys Compd.*, 2010, **489**, 167–169.
61 Y. Yang, X. W. Sun, B. K. Tay, J. X. Wang, Z. L. Dong and H. M. Fan, *Adv. Mater.*, 2007, **19**, 1839–1844.
62 Y. Yang, R. Scholz, H. J. Fan, D. Hesse, U. Gösele and M. Zacharias, *ACS Nano*, 2009, **3**, 555–562.
63 S. A. Mayén-Hernández, G. Torres-Delgado, R. Castanedo-Pérez, M. G. Villarreal, A. Cruz-Orea, J. G. M. Alvarez and O. Zelaya-Angel, *J. Mater. Sci.: Mater. Electron.*, 2007, **18**, 1127–1130.